Nanoscale zoom tomography with hard x rays using Kirkpatrick-Baez optics

R. Mokso, P. Cloetens, Eric Maire, Wolfgang Ludwig, Jean-Yves Buffiere

Nanoscale zoom tomography with hard x rays using Kirkpatrick-Baez optics

R. Mokso and P. Cloetens[a)]
European Synchrotron Radiation Facility (ESRF), F-38043 Grenoble, France

E. Maire, W. Ludwig, and J.-Y. Buffière
Matériaux Ingénierie Science MATEIS, INSA de Lyon, F-69621 Villeurbanne, France

(Received 16 December 2006; accepted 2 March 2007; published online 5 April 2007)

To overcome the limitations in terms of spatial resolution and field of view of existing tomography techniques, a hard x-ray projection microscope is realized based on the sub-100-nm focus produced by Kirkpatrick-Baez optics. The sample is set at a small distance downstream of the focus and Fresnel diffraction patterns with variable magnification are recorded on a medium-resolution detector. While the approach requires a specific phase retrieval procedure and correction for mirror imperfections, it allows zooming nondestructively into bulky samples. Quantitative three-dimensional nanoscale microscopy is demonstrated on an aluminum alloy in local tomography mode. © *2007 American Institute of Physics*. [DOI: 10.1063/1.2719653]

The improvement of spatial resolution triggered by a broad spectrum of materials science and biological applications is certainly one main driving force toward innovative designs and techniques in today's imaging technologies. This is particularly true for techniques that provide three-dimensional (3D) information about the sample in a nondestructive manner. X-ray tomography is the oldest among them and yet still evolving.[1,2] The use of Fresnel zone plates as objective lens has brought resolutions in the 100 nm range[3–5] and is most applied in the soft x-ray regime for the study of thin and light materials such as single cells. The emerging field of coherent diffraction imaging, based on phasing a coherent Fraunhofer diffraction pattern, is expected, in the 3D imaging of tiny isolated objects, to overcome the resolution limit set by the x-ray optical devices.[6] A drawback of the improved spatial resolution is the corresponding decrease in field of view and sample size (<10 μm). Larger, millimeter sized samples can be investigated in 3D with parallel beam synchrotron radiation microtomography, but in this case the resolution is limited by detector technology to slightly better than 1 μm. In this letter we present a projection microscope that bridges the gap in terms of resolution and specimen size between these nanoscale and microscale 3D imaging methods. It is based on state-of-the-art focusing of hard x rays characterized by a large penetration power and depth of focus. This allows exploring nondestructively in a three-dimensional manner bulk material at the nanoscale. The high flux makes it adapted to fast imaging for dynamical studies. Further improvement of spatial resolution does not necessarily imply a reduced efficiency as it is the case for imaging with Fresnel zone plates and high resolution detectors.

In the original tomography setup sketched on Fig. 1 bent graded multilayers set in the Kirkpatrick-Baez (KB) geometry focus undulator radiation to a spot below 90 nm in both directions.[7] They preserve a very high quasi-monocromatic flux (5×10^{11} photons/s with a medium monochromaticity $\Delta E/E\approx10^{-2}$). The sample is set at a small distance z_s (10–100 mm) downstream of the focal plane and a magnified Fresnel diffraction pattern is recorded on a medium-resolution detector set at a large distance z_d (several meters) from the sample. Changing z_s allows us to vary the magnification of the system, but will at the same time modify the nature of the image as it determines the effective propagation distance. The focusing device generates a spherical wave illumination of the sample. This geometry relates to a plane wave illumination through the equivalent propagation distance D and the magnification M given by the simple relations

$$D=\frac{z_s z_d}{z_s+z_d} \text{ and } M=\frac{z_s+z_d}{z_s}. \quad (1)$$

In the case of large magnification ($z_s \ll z_d$), the equivalent propagation distance is essentially equal to z_s. In the parallel beam geometry ($z_s \gg z_d$), the magnification is close to unity and the equivalent propagation distance $D\approx z_d$. Projection microscopy is therefore a magnified version of holotomography,[8,9] but it can also be considered as coherent diffraction imaging with a curved wave front.[10]

For all the projection microscopy the energy was set to 20.5 keV (wavelength $\lambda=0.06$ nm), corresponding to the third harmonic of the 32 mm period undulator of the ESRF beamline ID19 located 145 m upstream of the KB device. The vertically focusing first optical element of the KB is coated with a graded multilayer, which serves as a monochromator and increases the acceptance angle of the system.

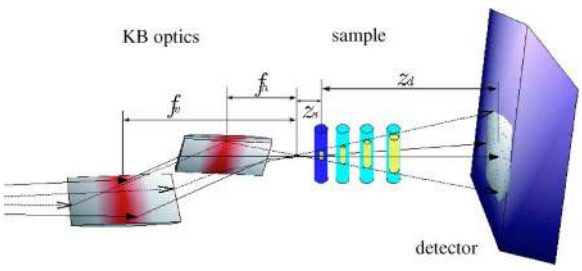

FIG. 1. (Color online) Scheme of the tomography setup using the divergent beam produced by Kirkpatrick-Baez optics.

[a)]Electronic mail: cloetens@esrf.fr

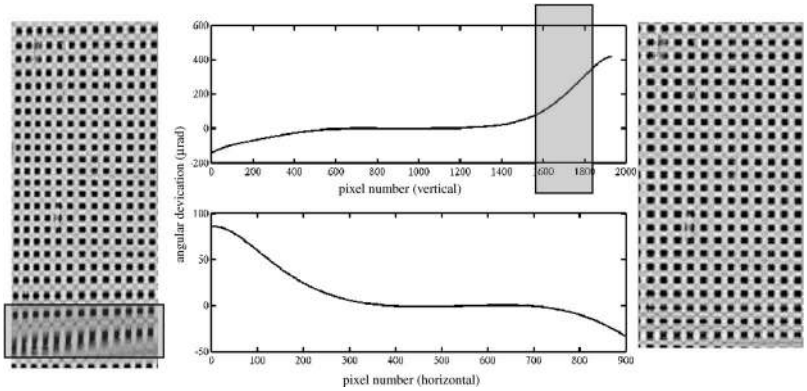

FIG. 2. Wave front characterization with a 2 μm period grid. Left, distorted image; middle top, vertical angular deviation as a function of the vertical pixel coordinate; middle bottom, horizontal angular deviation as a function of the horizontal pixel coordinate; right, same grid image after correction of the distortions. The optical figure errors increase toward the edges of the mirrors.

The opening angles of the cone beam are 2 and 3.5 mrad in the horizontal and vertical directions, respectively, crucial parameters for imaging as they determine the field of view for a given focus-to-sample distance. The projection radiographs are recorded at a fixed distance z_s+z_d of 3.9 m from the focal plane using an x-ray detector consisting of a $Gd_2O_2S:Tb$ scintillator, a fast readout low noise charge coupled device (CCD) based camera, and visible light optics with an effective pixel size of 7.46 μm. The typical exposure time using the maximal dynamic range of the 14 bit CCD camera is 1 s per radiograph. For a tomographic scan 900 such images with $1024(h)\times 2048(v)$ illuminated pixels are recorded. During our experiments the synchrotron ring was operating in low-current mode; therefore, the exposure time could be further reduced, indicating the high efficiency as one of the critical advantages of the present KB based projection geometry. Keeping the scanning time shorter relieves the requirements on the temporal stability of the sample as well as of the imaging system itself.

A single radiograph can be recorded with a spatial resolution better than 100 nm, but the resolution in tomographic mode is generally worse and much effort is needed to keep it close to the original value. Before applying the three-dimensional reconstruction itself, individual images must undergo preprocessing to obtain *projections* of the sample. A first correction is related to the figure errors of the reflecting surfaces resulting in deviations with respect to a spherical wave of the sample illumination. In first approximation they induce a geometrical distortion of the images. Two-dimensional grids (silicon phase gratings of 2 and 3 μm period) are used as simple wave front sensors. At the end of the tomographic acquisition the grids are imaged at the same distance z_s. By registering the positions of the maxima and minima of the grid images and employing a pure geometrical optics approach, the angular displacements of the real extrema compared to the ideal grid image are determined. This information is used to undistort the radiographs by means of interpolation techniques (see Fig. 2).

Due to propagation, a single radiograph is a Fresnel diffraction pattern determined both by the attenuation and phase modulation introduced by the object. To disentangle the object information radiographs are recorded corresponding to different focus-to-sample distances. More than two values of z_s are required in practice for reliable phase retrieval due to intrinsic properties of Fresnel diffraction patterns, a single pattern at equivalent propagation distance D being blind to the spatial frequencies $\sqrt{p/(\lambda D)}$ of the phase modulation for all natural numbers p. After bringing the undistorted images to the same magnification and origin, we obtain in-line holograms of the sample as in the parallel beam case. To these we apply the phase retrieval algorithms[8] modified for the KB geometry. The modification merely involves the incorporation of relations (1) that formalize the equivalence between cone and parallel beam geometry. This approach is illustrated in Fig. 3 on a flat sample consisting of freeze-dried neuron cells on a 2 μm thick polymer film. Figures 3(a) and 3(b) are radiographs after correction for the mirror distortions but before bringing them to the same maximum magnification as radiograph (c). The result of the phase retrieval procedure is

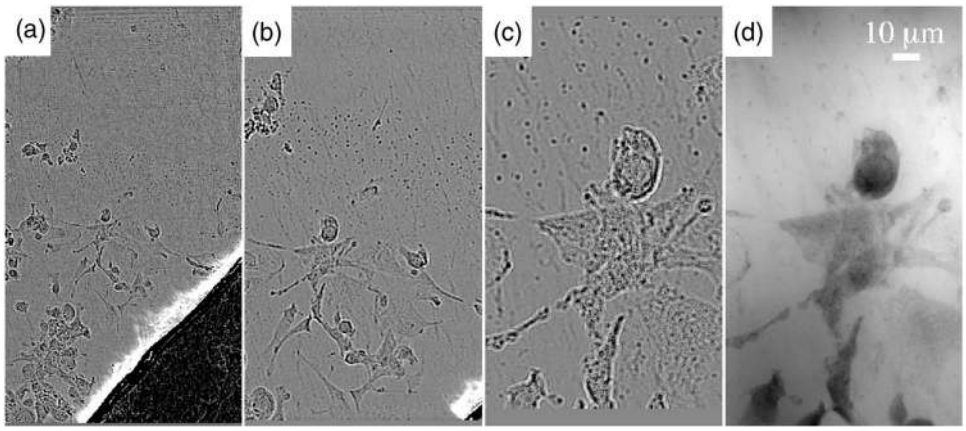

FIG. 3. Magnified radiography of a freeze-dried neuron cell demonstrating the effect of the sample-to-focus distance z_s on the magnification M and equivalent propagation distance D. The radiographs were recorded at z_s of (a) 225 mm, 175 mm, (b) 125 mm, 75 mm and (c) 45 mm. Combining numerically five radiographs a phase map (d) with a pixel size of 85 nm is retrieved.

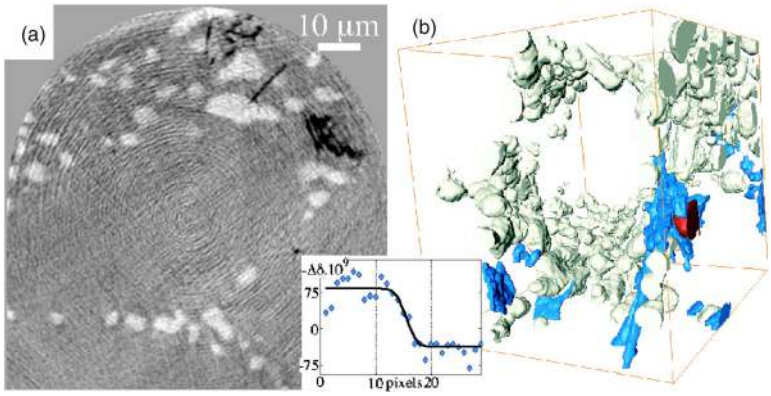

FIG. 4. (Color online) (a) Tomographic slice of an Al–Si alloy. Inset: Profile of the changes in refractive index. (b) Rendering of a 45 μm large extracted volume showing silicon particles (bright), a pore (red), and iron rich inclusions (blue).

shown in Fig. 3(d). The original algorithm uses five distances, three of which are shown in Fig. 3, and assumes the object to be a pure phase object. Phase retrieval is necessary in this geometry to improve the spatial resolution that would be otherwise degraded by the presence of the diffraction pattern.

The retrieved phase maps now constitute projections of the object and therefore the correct input for a tomographic reconstruction. Magnified tomographic imaging is useful for the three-dimensional determination of the internal microstructure of materials, as demonstrated here on cast aluminum-silicon samples. Tomographic scans of large 1 mm diameter samples were recorded at five distances corresponding to magnifications $M=\{15;20;30;58;83\}$. This results in a final voxel size of 90 nm and a field of view of approximately 90 μm, i.e., more than ten times smaller than the sample size. This local or zoom tomography mode keeps the specimen preparation straightforward as it is not necessary to prepare very thin (diameter of 50–100 μm) specimens. Working on bulky samples is also more relevant from the application point of view, for instance, for *in situ* experiments.[11] The reconstructions were performed using the filtered back-projection algorithm for the parallel beam case. This is a first approximation justified by the small divergence of the beam not exceeding 3.5 mrad. The slice reconstructed from the phase projections [Fig. 4(a)] is a quantitative representation of the local refractive index which is proportional to the electron density. The linear attenuation coefficients of aluminum and silicon differ very little; therefore, coherent imaging offers a better tool than attenuation to distinguish the two components in the bulk of the alloy. From a line profile through a silicon particle edge the spatial resolution is estimated to be 290 nm. It is limited at present by the mechanical precision of the rotation stage, the mirror distortions, and artifacts due to local tomography. The dominant artifacts visible in the reconstructions are ring shaped and attributed to imperfect correction of the background image introduced by the KB optics. This correction is done by the so-called flat-field correction which consists in dividing the image intensity with and without sample and does not take into account any wave phenomena. This approximation fails when strong refraction effects occur as it is the case near the boundaries of structures. This "lens effect" makes the investigation of narrow samples not exceeding the field of view at present impossible, but it is not perturbing on nearly flat samples as in Fig. 3. The quality of the tomographic data is sufficient to correctly segment the different phases of the alloy. The volume rendering in Fig. 4(b) reveals the presence of silicon particles (bright), and also a pore (red) and iron rich particles (blue), as expected from the composition and processing of the material. The complex spatial distribution of the silicon particles is typical of the cast dendritic structure of this alloy and can generally not be determined from two-dimensional imaging techniques. The measured difference in refractive index between Al and Si is 0.13×10^{-6}, very close to the expected value of 0.14×10^{-6} for pure Al–Si. The measurement for the intermetallic phase (density $\approx$3.3 g/cm^3) allows us to identify it as being Al_5FeSi. The most commonly reported compositions of iron rich particles in this alloy are Al_5FeSi and Al_8Fe_2Si. This example illustrates the feasibility of submicrometer resolution quantitative tomography on bulky and engineering samples using a divergent beam and phase retrieval. The high flux in this configuration could be exploited for shortening the acquisition time and studying dynamic processes.

The authors would like to thank Ch. David (Paul Scherrer Institute) for providing the silicon grids and R. Ortega (CNRS, Gradignan) for the neuron cell sample.

[1] C. S. Schroer, J. Meyer, M. Kuhlmann, B. Benner, T. F. Gunler, B. Lengeler, C. Rau, T. Weitkamp, A. Snigirev, and I. Snigireva, Appl. Phys. Lett. **81**, 1527 (2002).
[2] S. Mayo, T. Davis, T. Gureyev, P. Miller, D. Paganin, A. Pogany, A. Stevenson, and S. Wilkins, Opt. Express **11**, 2289 (2003).
[3] C. A. Larabell and M. A. L. Gros, Mol. Biol. Cell **15**, 957 (2004).
[4] G. C. Yin, M. T. Tang, Y. F. Song, F. R. Chen, K. S. Liang, F. W. Duewer, W. Yun, C. H. Ko, and H. P. D. Shieh, Appl. Phys. Lett. **88**, 241115 (2006).
[5] H. Toda, K. Uesugi, A. Takeuchi, K. Minami, M. Kobayashi, and T. Kobayashi, Appl. Phys. Lett. **89**, 143112 (2006).
[6] I. K. Robinson and J. W. Miao, MRS Bull. **29**, 177 (2004).
[7] O. Hignette, P. Cloetens, G. Rostaing, P. Bernard, and C. Morawe, Rev. Sci. Instrum. **76**, 063709 (2005).
[8] P. Cloetens, W. Ludwig, J. Baruchel, D. V. Dyck, J. V. Landuyt, J.-P. Guigay, and M. Schlenker, Appl. Phys. Lett. **75**, 2912 (1999).
[9] P. Cloetens, R. Mache, M. Schlenker, and S. Lerbs-Mache, Proc. Natl. Acad. Sci. U.S.A. **103**, 14626 (2006).
[10] K. A. Nugent, A. G. Peele, H. N. Chapman, and H. M. Quiney, Acta Crystallogr., Sect. A: Found. Crystallogr. **61**, 373 (2005).
[11] J. Y. Buffière, E. Maire, P. Cloetens, G. Lormand, and R. Fougères, Acta Mater. **47**, 1613 (1999).